Invited Articles

Particle-induced viscous fingering: Review and outlook

Rui Luo, Yun Chen, and Sungyon Lee*
Department of Mechanical Engineering, University of Minnesota, Minneapolis, Minnesota 55455, USA

(Received 29 June 2018; published 21 November 2018)

Changes in bulk rheology of suspensions with the particle concentration are well documented, ranging from normal stress differences to shear-thinning and shear-thickening behaviors. However, relatively little is known about the impact this bulk rheology can have on the interfacial dynamics of free-surface, particle-laden flows. Recently, it has been demonstrated that particles suspended in liquid may cause viscous fingering by modifying the local rheology near the fluid-fluid interface, when a mixture of noncolloidal particles and viscous oil displaces air inside a Hele-Shaw cell. As the same flow configuration sans particles is inherently stable to viscous fingering, the simplicity of the baseline flow renders this a perfect model problem to study to gain insight into the coupling between the bulk rheology and fluid-fluid interface. To that end, we first summarize the recent experimental findings of this particle-induced viscous fingering, which highlights the effect of the particle volume fraction and the particle diameter relative to the gap size on the emergent finger geometries. We also present experimental measurements of the critical viscosity gradient at the fingering onset, as well as the surprising time-independent finger growth regime for sufficiently large volume fractions. These results—both old and new—together highlight the similarities as well as important differences between fingering in suspensions versus pure liquid, suggesting a direction for continued research at the intersection between suspension rheology and interfacial dynamics.

DOI: 10.1103/PhysRevFluids.3.110502

I. INTRODUCTION

Solid particles suspended in a viscous liquid fundamentally change the dynamics of the bulk mixture, leading to the rise in the effective viscosity and other rheological changes that become pronounced at moderate to dense particle concentrations [1,2]. The pioneering work of Leighton and Acrivos [3,4] has yielded a flurry of studies on the dynamics of particle-laden flows in the low-Reynolds-number and large-Péclet-number limits (e.g., see Ref. [5]). In particular, non-Brownian particles under shear are observed to migrate across streamlines from the regions of high to low shear stress. This so-called shear-induced migration stems from both hydrodynamic and nonhydrodynamic close interactions between particles [3,4,6]. As particle concentrations increase, suspensions exhibit highly non-Newtonian behaviors, ranging from shear-thinning, normal stress differences, all the way to a jamming transition that leads to a divergence in viscosity [1,2,7]. More recently, the onset of shear thickening in dense suspensions has been shown to result from the transition from lubricated to frictional interparticle contact and remains an active area of research, which is directly applicable to suspension processing [8–14].

Through their impact on the bulk rheology, suspended particles can also alter the dynamics of the fluid-fluid interface. In fact, researchers have used the free surface shapes of suspensions to measure the second normal-stress difference, based on the classical rheometry techniques of complex liquids.

*sungyon@umn.edu

For instance, the well-known rod-climbing behavior of a viscoelastic fluid is caused by the rise in normal stress differences and has led to the invention of rotating-rod rheometry. Analogously, the decrease in normal stress differences in suspensions under shear leads to the rod-dipping behaviors, and the subsequent interfacial shape is measured to infer the rheology of the given suspension [15]. Similarly, inspired by the works of Wineman and Pipkin [16] and Tanner [17], Couturier and colleagues [18] used the free surface shapes of the particle-laden flow through an open tilted trough to measure the second normal-stress difference of the given mixture.

In the aforementioned studies, the free surface shape is considered the convenient *by-product* of the bulk suspension rheology but not the focus of the study itself. So far, only a limited number of studies have examined the coupling between bulk suspensions and fluid-fluid interfaces, despite how common free-surface, particle-laden flows are. This offers an opportunity to formulate new research questions in a wide array of fluid mechanics problems. For instance, particles suspended in a viscous liquid are shown to accelerate the droplet pinch-off [19–24], as the diameter of the thinning liquid thread becomes comparable to the particle size. In another example, the suppression of fingering is reported at high particle concentrations, in gravity-driven, free-surface flows of a glass particle and oil mixture down an incline [25–34]. More recently, Kulkarni and colleagues [35] showed that the fingering instability of the thin spreading suspension film under rotation has a nonmonotonic dependence on the particle concentration.

Even with the limited examples, one can clearly see a diverse set of flow configurations in which suspended particles substantially alter the dynamics of the suspension-gas interface. Furthermore, the role of suspended particles to either suppress or to accelerate the interfacial instability appears as varied as the flow type itself. This is in clear contrast with the well-developed area of particle adsorption or trapping on the fluid-fluid interface. Here, through capillary interactions, particles are shown to stabilize the interface against breakage in various configurations ranging from particle rafts [36–40], particle-stabilized emulsions [41], to armored droplets [42–44] and liquid/gas marbles [45,46]. While it may not be plausible to come up with similar unifying principles for suspended particles, we can start by simplifying the present problem at hand. For instance, what has further complicated the previous studies on free-surface, particle-laden flows is the complexity of the baseline particle-free flows that are susceptible to interfacial instabilities. Hence, we will presently focus on a seminal free-surface flow that is inherently stable to viscous fingering: injection of viscous oil into a Hele-Shaw cell that is open to air. That way, any deviation of the free surface from a stable circular shape may be attributed to the presence of particles inside the mixture.

When noncolloidal particles are added to the viscous oil that displaces air, viscous fingering emerges even in the absence of the destabilizing viscosity ratio between the invading and defending fluids. This surprising instability was first observed by Tang and colleagues [47] and later in a squeeze flow by Ramachandran and Leighton [48]. More recent studies from our group [49,50] systematically demonstrated the dependence of the resultant fingering on the particle concentration as well as on the particle size. We have found that the key to this particle-induced viscous fingering is the change in local rheology near the interface, as particles preferentially enrich the expanding meniscus due to shear-induced migration. This change in rheology then causes miscible fingering inside the suspension and, subsequently, interfacial deformations that are unobserved in the pure liquid counterpart. Therefore, through this model problem, we will emphasize how the particle dynamics in the bulk can lead to new phenomena at the fluid-fluid interface.

The paper is organized as follows. In Sec. II, we first summarize the recent experimental results of Refs. [49,50] and the fundamental mechanism behind this particle-induced viscous fingering. Then, Sec. III consists of two new important findings: the existence of critical viscosity gradient at the fingering onset and the saturation behavior in finger growth. In particular, these new experimental results are used to highlight the striking analogy as well as clear differences between the current problem and miscible fingering in liquids. We conclude the paper in Sec. IV with the summary and outlook into new research questions prompted by the current study.

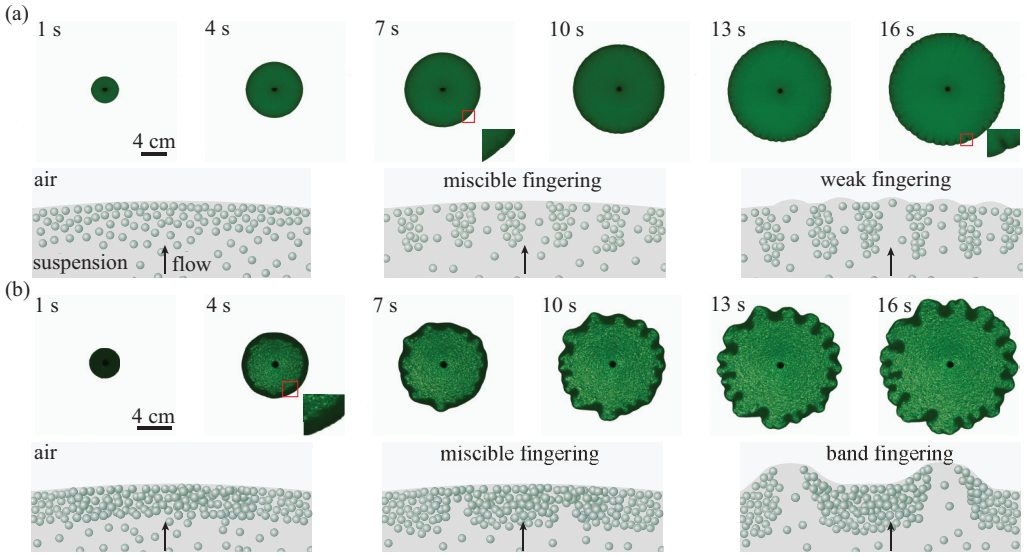

FIG. 1. Time-sequential images of two representative experiments with corresponding schematics to highlight the key physical picture. (a) $\phi_0 = 0.28$ and $h/d = 10.2$ (weak fingering): Particles first collect on the interface, causing miscible fingering. Miscible fingering is evidenced by the formation of particle clusters normal to the growing interface. Then, the interfacial fingers form between them. (b) $\phi_0 = 0.30$ and $h/d = 2.2$ (band fingering): Particles are shown to clearly form a sharp band on the interface, which first grows radially but starts to break around 7 s; this causes larger interfacial deformations especially compared to weak fingering in panel (a).

II. PARTICLE-INDUCED VISCOUS FINGERING

When the suspension of noncolloidal particles and viscous oil radially displaces air in a Hele-Shaw cell, viscous fingering is observed at the suspension-air interface. First reported by Tang *et al.* [47], this phenomenon is counterintuitive at the outset since the viscosity ratio between the invading suspension and displaced air is inherently stable to viscous fingering [51]. However, the time-sequential images of the experiments in Fig. 1 reveal that this interfacial instability originates from the particle dynamics inside the bulk suspension, which results in the destabilizing viscosity gradient. Hence, understanding this instability must start by understanding what happens inside the bulk suspension.

In Fig. 1(a), one can observe the accumulation of particles near the interface, indicated by a slightly darker region. Here, the ratio of gap thickness h to the particle diameter d corresponds to 10.2, while the particle volume fraction is $\phi_0 = 0.28$. Following accumulation, particles form clusters perpendicular to the interface, which couple to small but clear interfacial deformations. Particle clusters and an interfacial finger that forms between them are more clearly shown in the inset image at $t = 16$ s. In Fig. 1(b) ($\phi_0 = 0.3$ and $h/d = 2.2$), the particle accumulation is evident immediately upon injection into the cell; the accumulated particles form a discrete "particle band" on the interface that first expands radially and then breaks around 7 s, causing pronounced interfacial deformations. The striking differences in the finger geometry in Figs. 1(a) and 1(b) must arise from the difference in h/d (i.e., 10.2 versus 2.2), as ϕ_0 remains close to 0.3 in both cases. Despite the differences, experiments in Figs. 1(a) and 1(b) follow the same basic processes leading to viscous fingering: particle accumulation that generates a destabilizing viscosity ratio, miscible fingering near the interface, and fingering of the suspension-air interface, as illustrated by the schematics accompanying each experiment.

Simply put, the key to particle-induced viscous fingering is the destabilizing viscosity gradient (less viscous fluid invading more viscous one) that is caused by the nonuniform distribution of

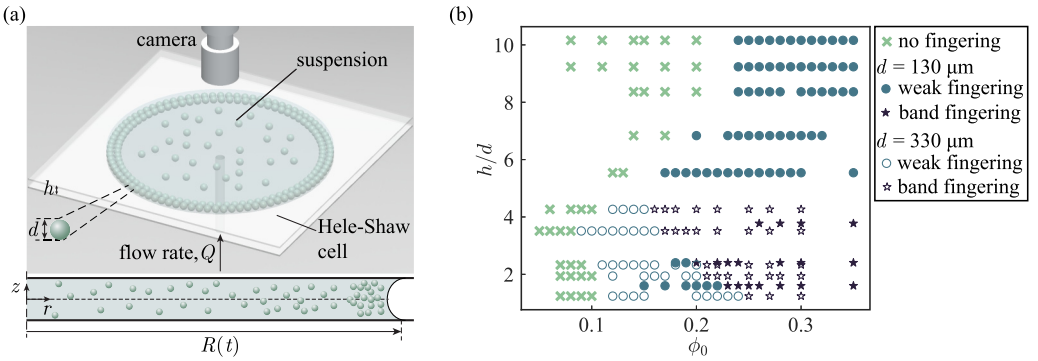

FIG. 2. (a) The schematic of the experimental setup shows the injection of suspension into a Hele-Shaw cell from the bottom center of the channel. The side-view schematic below includes the radial r and normal z coordinates, as well as the location of the evolving suspension-air interface $R(t)$. (b) The phase diagram summarizes all the experimental results of Refs. [49,50] to show "no fingering," "weak fingering," and 'band fingering" regimes as a function of ϕ_0 and h/d.

particles. For instance, the destabilizing viscosity gradient can be generated by injecting pure oil into the oil-particle mixture, which leads to miscible viscous fingering (work currently under way). This is an extension of previous studies in which particle-modified immiscible fingering is observed upon the injection of air into a suspension [52–55]. However, uniquely in the current setup, particles self-organize inside the suspension and naturally set the destabilizing viscosity gradient by accumulating on the interface. In addition, the stabilizing suspension-air interface plays a crucial role in particle dynamics and the onset and growth of fingering. Hence, this coupling between the the bulk suspension rheology and the interfacial dynamics is at the center of the particle-induced viscous fingering.

A. Experiments

As illustrated in the schematic in Fig. 2(a), all the experiments [49,50] have been conducted in a Hele-Shaw cell consisting of two Plexiglass plates ($30.5 \times 30.5 \times 3.8$ cm) that are separated to a gap thickness $h = 0.2$–1.4 mm with shims. The mixture of noncolloidal particles (density $\rho_p = 1.00\,\mathrm{g/cm^3}$, Cospheric) and silicone oil (density $\rho_l = 0.96\,\mathrm{g/cm^3}$, viscosity $\mu_l = 0.096$ Pa s) is injected into the center of the cell through the hole in the bottom plate at a fixed flow rate $Q = 30$–150 mL/min via a syringe pump (New Era). As the monodisperse suspension spreads radially out between the two plates, a digital camera (Cannon 60D, 1920×1080 pixel images, FOV 64°) records the particle-laden flow from the top down, with uniform illumination provided by an LED panel (EnvirOasis) from below. The two major parameters varied in the experiments are the particle volume fraction $\phi_0 = 0.05$–0.35 and the gap thickness relative particle diameter, $h/d = 1.2$–10.2. The latter is varied by incrementally changing h and also by switching between two sets of polyethylene particles with average diameters, $d = 330$ and $130\,\mu$m, respectively. More details about the experimental setup can be found in Refs. [49,50].

We hereby combine the experimental results of Refs. [49,50] into a single phase diagram in terms of ϕ_0 and h/d in Fig. 2(b). There are three major observations to be made here. First, regardless of the value of h/d, for sufficiently low ϕ_0, the suspension interface remains circular and stable on the length and timescale of the experimental run. We term this "no fingering" regime and mark it with an "x" symbol in Fig. 2(b). As ϕ_0 is increased from this stable low-ϕ_0 limit, gradual accumulation of particles is observed near the interface. This accumulation eventually leads to the formation of particle clusters and interfacial deformations, as previously shown in Fig. 1(a). This regime is termed "weak fingering" (marked with an "o"). Lastly, for $h/d < 5$ and sufficiently large ϕ_0, we observe a more pronounced interfacial instability which results from the formation and breakup of the discrete particle band. This so-called "band fingering" regime was previously illustrated in Fig. 1(b). Notably,

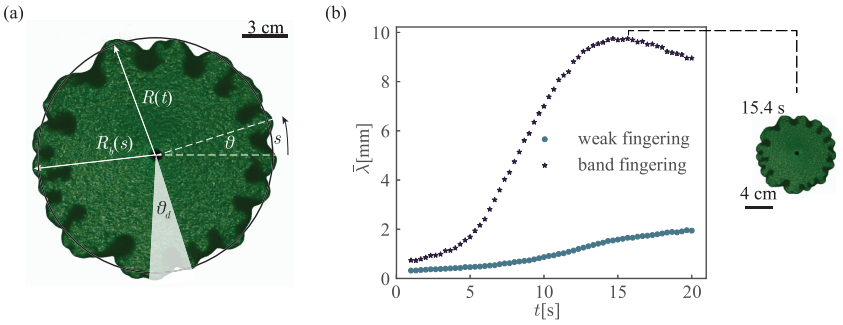

FIG. 3. (a) The suspension-air interface is described following a curvilinear coordinate s. The instantaneous distance from the center to any arbitrary point on the interface is denoted as $R_b(s)$, while R is the radius of the best fitted circle out of all points along the interface. We identify local max (R_b) and min (R_b) inside the small "wedge" defined by θ_d; then, the characteristic finger length $\bar{\lambda}$ is computed by averaging max (R_b) − min (R_b) over the entire interface. (b) The plot of $\bar{\lambda}$ over time t quantitatively illustrates the difference between band fingering ($\phi_0 = 0.3,\ h/d = 2.2$) and weak fingering ($\phi_0 = 0.28,\ h/d = 10.2$). In addition to being larger in magnitude, there is a peak in $\bar{\lambda}$ for band fingering that corresponds to the moment of band breakup; $\bar{\lambda}$ increases gradually in the weak fingering case.

experiments with two different values of d collapse in the ϕ_0-h/d phase diagram [Fig. 2(b)]; this demonstrates that fingering regimes are correctly determined by h/d and ϕ_0 alone.

To illustrate quantitative differences between the fingering regimes, we plot the characteristic finger length $\bar{\lambda}$ over time t in Fig. 3(b) for band fingering ($\phi_0 = 0.3,\ h/d = 2.2$) and weak fingering ($\phi_0 = 0.28,\ h/d = 10.2$). With R_b denoting the instantaneous distance between the center and the interface [schematic in Fig. 3(a)], we first compute the difference between the local extrema in R_b, or max (R_b) − min (R_b), inside a small "wedge" defined by θ_d. The value of θ_d is determined empirically for each experiment based on the number of fingers that are observed. Then, the characteristic finger length $\bar{\lambda}$ is determined by averaging max (R_b) − min (R_b) along the entire interface, s. As shown in Fig. 3(b), the magnitude of $\bar{\lambda}$ is almost an order of magnitude larger for band fingering. More important, in band fingering, the peak in $\bar{\lambda}$ corresponds to the moment at which the particle band first breaks, yielding large interfacial deformations. Following the band breakup, the interface tends to recover the circular shape, which causes to $\bar{\lambda}$ decrease. By contrast, the rise in $\bar{\lambda}$ in weak fingering is gradual and subtle, rendering its exact onset much more difficult to pin down based on $\bar{\lambda}$. We will revisit this elusive nature of weak fingering in Sec. III.

For completeness, we emphasize that our definition of a particle band has two key features. First, the increase in particle concentration occurs *sharply* rather than *gradually* near the interface. This formation of the sharp particle band is unique to $h/d < 5$, which will be addressed in Sec. II B. Second, the particle volume fraction inside the band, or ϕ_b, must be very dense, so that the band's response to the incoming flow is inherently different from the dilute suspension. The experimental measurement in Ref. [50] has shown that ϕ_b is approximately 0.5, which is close to the jamming limit only when $h \sim d$. The latter is the key to enhanced interfacial deformations that are observed in band fingering. Notably, we also observe pronounced interfacial deformations even for $h/d > 5$ as long as $\phi_0 > 0.3$, as the dense suspension must reach the maximum packing fraction near the interface. However, they are not preceded by the formation of the sharp particle band and, hence, are not noted as "band fingering" on the phase diagram.

B. Key to fingering: Particle accumulation

Whether it leads to weak or band fingering, the first step to particle-induced viscous fingering is the particle accumulation at the fluid-fluid interface. To uncover the source of meniscus enrichment, we begin by considering the flow far upstream of the interface. The particle $\boldsymbol{v}^{\mathrm{p}}$ and mixture velocities

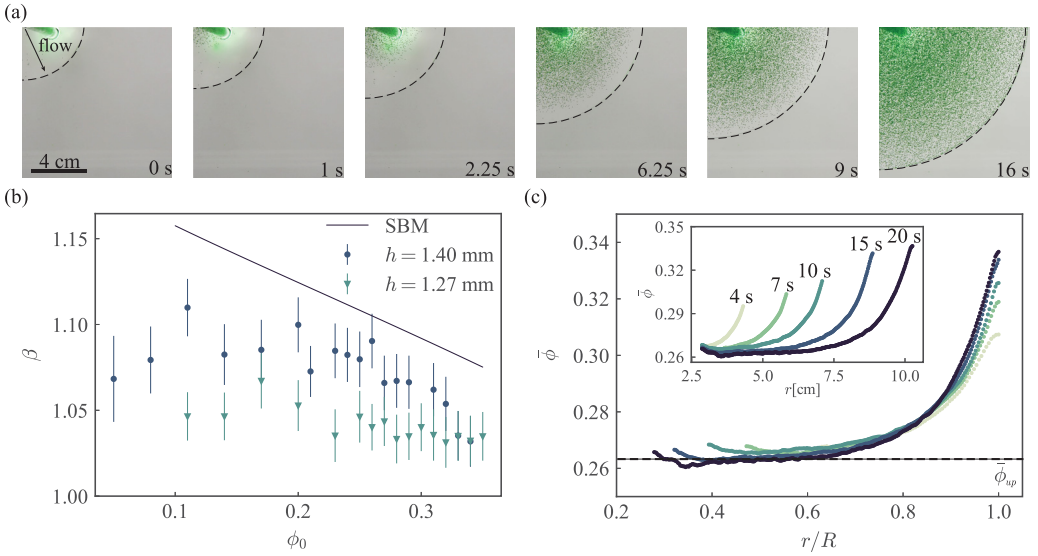

FIG. 4. (a) Even when clear oil is injected ahead of the suspension, particles catch up to the interface, demonstrating that particles move faster than the mixture on average, or $\bar{u}_r^{\mathrm{p}} > \bar{u}_r$. (b) The plot of the ratio of average velocities β as a function of ϕ_0 includes the calculation result of the suspension balance model (SBM) in a solid line, as well as the experimental measurement for $h = 1.40$ and 1.27 mm. (c) The particle accumulation is evidenced in the plot of $\bar{\phi}$ over r/R for $\phi_0 = 0.28$ and $h/d = 10.2$; the dotted line indicates the depth-averaged concentration in the upstream regime, $\bar{\phi}_{\mathrm{up}}$.

$\boldsymbol{v}$ are related by $\boldsymbol{v} = (u_r, u_\theta, u_z) = \phi \boldsymbol{v}^{\mathrm{p}} + (1-\phi)\boldsymbol{v}^{\mathrm{f}}$ in the continuum sense, where $\boldsymbol{v}^{\mathrm{f}}$ is the fluid velocity. As the suspension moves radially out upon injection, particles tend to preferentially focus at the channel centerline ($z = 0$) where shear vanishes, away from the channel walls ($z = \pm h/2$), to reduce particle collisions. Known as shear-induced migration [3,4,6], this cross-stream migration of noncolloidal particles from regions of high to low shear yields higher particle concentration at $z = 0$, where the flow is fastest. Consequently, the average particle velocity in the radial direction $\bar{u}_r^{\mathrm{p}}$ must be greater than the case of uniform dispersion, as well as the average mixture velocity $\bar{u}_r$. To illustrate this, the depth-averaged particle and mixture velocities in r are given by

$$\bar{u}_r^{\mathrm{p}} = \frac{1}{h\bar{\phi}} \int_{-h/2}^{h/2} \phi(z) u_r^{\mathrm{p}}(r, z)\, dz, \qquad \bar{u}_r = \frac{1}{h} \int_{-h/2}^{h/2} u_r(r, z)\, dz, \tag{1}$$

where $\bar{\phi} = \int_{-h/2}^{h/2} \phi(z)\, dz/h$ is the depth-averaged particle concentration. Note that $\bar{u}_r^{\mathrm{p}} = \bar{u}_r$, if $\phi(z) = \bar{\phi} =$ constant in z. Hence, if there are more particles at $z = 0$ due to shear-induced migration, one can readily see that $\bar{u}_r^{\mathrm{p}} > \bar{u}_r$.

This higher particle velocity relative to that of the mixture is the key to particle accumulation on the fluid-fluid interface. Based on mass conservation, the fluid-fluid interface expands radially with the mixture at $\bar{u}_r|_R = Q/(2\pi Rh)$, where $R(t)$ is the radial position of the interface. Hence, if $\bar{u}_r^{\mathrm{p}} > \bar{u}_r$, the particles from upstream must eventually catch up to the interface, which acts as an impermeable wall. This is clearly demonstrated by experimentally injecting clear oil ahead of the suspension. As shown in Fig. 4(a), particles are observed to catch up to the oil-air interface over time, which shows that $\bar{u}_r^{\mathrm{p}} > \bar{u}_r$. Hence, the origin of particle accumulation lies in shear-induced migration of particles in the z direction and the presence of the fluid-fluid interface to "collect" incoming particles. However, *how* the particles collect—gradually or sharply—must depend on the flow profiles near the interface.

Even without particles, the fluid flow near the expanding interface is inherently more complex than the unidirectional flow upstream. Near the interface, a secondary flow known as a "fountain flow" [56] allows the parabolic upstream flow to transition into a plug flow on the meniscus. While neglecting the effects of particles, this flow can be qualitatively described by the following stream function ψ [57]:

$$\psi = \frac{Qz^*}{4\pi}(1 - 4z^{*2})[1 - \exp(y^*\sqrt{6})], \tag{2}$$

where $z^* = z/h$ is the dimensionless vertical coordinate, while $y^* = (r - R)/h$ corresponds to the dimensionless radial coordinate defined from the interface. In the frame moving with the expanding interface, the fountain flow reverses the direction at a distance h_w from the walls and moves away from the interface; h_w can be easily computed from ψ as $h_w \sim h/5$ (details in the Supplemental Material for Ref. [50]). Then, when $d < h_w \sim h/5$, particles that come toward the interface may get entrained into the reverse flow near the wall, leading to the gradual particle accumulation at the interface. By the same token, particles whose diameter d is larger than h_w are more likely to simply collect on the interface, resulting in a shocklike formation of the particle band. This simple scaling helps rationalize the emergence of the band formation for $h/d < 5$; more details about the band formation and fingering onset can be found in Ref. [50].

Going back to the minimum ingredient for accumulation, we hereby define the ratio of average particle to mixture velocities, $\beta \equiv \bar{u}_r^{\mathrm{p}}/\bar{u}_r$, which needs to be at least greater than 1 for accumulation to occur. The limit of $\beta = 1$ would correspond to the case of uniform dispersion with no shear-induced migration. When we combine Eq. (1) with the following constant injection conditions,

$$Q = 2\pi r \int_{-h/2}^{h/2} u_r \, dz, \qquad Q\phi_0 = 2\pi r \int_{-h/2}^{h/2} u_r^{\mathrm{p}} \phi \, dz, \tag{3}$$

the expression for β simply reduces to $\phi_0/\bar{\phi}_{\mathrm{up}}$; here, the subscript "up" has been added to emphasize the validity of β strictly in the upstream region. In addition, this minimum accumulation condition, $\beta = \phi_0/\bar{\phi}_{\mathrm{up}} > 1$, makes sense in terms of mass conservation: There must be particle depletion in the upstream (i.e., $\bar{\phi}_{\mathrm{up}} < \phi_0$) to account for higher particle concentration near the interface.

The plot of β versus ϕ_0 is included in Fig. 4(b), which combines both the theoretical and experimental results from Ref. [49]. The experimental value for $\beta = \phi_0/\bar{\phi}_{\mathrm{up}}$ is straightforward to compute as $\bar{\phi}_{\mathrm{up}}$ can be extracted from the light intensity I of the top-down experimental images, or $\bar{\phi} = k \log(I/I_{\min})/\log(I/I_{\max})$. Here, $I_{\min}$ and $I_{\max}$ correspond to the minimum and maximum intensity values of the given image, respectively [58]. The empirical parameter k is computed by ensuring mass conservation, such that $2\pi \int_{\delta}^{R} \bar{\phi}(r) r \, dr = \pi\phi_0 R^2$, where δ accounts for the injection tube. Assuming axisymmetry, $\bar{\phi}$ is averaged from $\theta = 0$ to 2π at given r. The resultant plot of $\bar{\phi}$ over r/R in Fig. 4(c) clearly demonstrates the gradual rise in the particle volume fraction toward the interface at $r/R = 1$. More important, $\bar{\phi}$ is shown to plateau at $\bar{\phi}_{\mathrm{up}}$ [dotted line in Fig. 4(c)] at a sufficient distance from the injection point and the interface, validating the quasi-fully-developed assumption in the upstream region.

The existence of the quasi-fully-developed regime allows us to calculate β theoretically within the continuum framework of the suspension balance model (SBM) [59]. The SBM [59] accounts for the rise in normal stress differences in the mixture of rigid particles and Newtonian liquid that are induced by shear; the model then captures shear-induced migration of particles that results from the normal stress gradient. We previously employed the lubrication approximations and equilibrium assumptions to calculate the velocity and particle concentration profiles in the upstream regime. From this simplified 1D model, the value of β can be computed numerically for given ϕ_0 (see Ref. [49] for the derivation). As evident in Fig. 4(b), the match between experiments and theory is far from perfect but is within reason especially for larger h, for which the continuum assumption is more appropriate. In addition, a significant deviation between theory and experiments is expected for low ϕ_0, as Snook and colleagues [60] recently demonstrated the inaccuracy of SBM in the dilute regime.

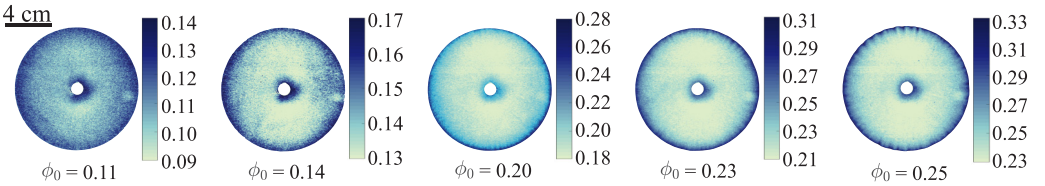

FIG. 5. Processed experimental images at the final time ($t = 18$ s) reveal the extent of particle accumulation at varying ϕ_0 at $h/d = 10.2$. The clear rise in $\bar{\phi}$ relative to ϕ_0 becomes evident for $\phi_0 > 0.14$, while miscible fingering and interfacial deformations are visible at $\phi_0 = 0.25$.

Even setting the deviation between theory and experiments aside, this plot of β-ϕ_0 in Fig. 4(b) is inconclusive at best, providing more questions than answers. As previously discussed, β is a conceptually useful parameter that can be readily measured and computed to show the effective range of shear-induced migration. However, the inaccuracy of β in the dilute regime renders $\beta \geqslant 1$ an impractical criterion for predicting the onset of particle accumulation. In fact, $\beta > 1$ for all ϕ_0 in Fig. 4(b), which misleadingly indicates that accumulation is expected for all ϕ_0. To demonstrate this, Fig. 5 consists of experimental images at $t = 18$ s that have been rescaled to highlight the particle distribution inside the suspension for $h/d = 10.2$. Here, particle accumulation is observed for ϕ_0 as low as 0.14 (more blue/higher $\bar{\phi}$ near the interface). Then, for $\phi_0 \gtrsim 0.2$, a thin, well-defined region of higher concentration emerges near the interface, separated by the fully developed region with constant concentration, $\bar{\phi}_{\text{up}} < \phi_0$. However, the onset of miscible fingering is not evident until $\phi_0 \gtrsim 0.23$. This clear gap between the onset of particle accumulation and the onset of miscible fingering naturally leads to a new question: "Why does no fingering occur despite the destabilizing viscosity gradient set by particle accumulation?" In order to address this question, we will experimentally characterize the conditions incipient to miscible fingering in Sec. III.

III. FROM PARTICLE ACCUMULATION TO FINGERING

To quantify the onset and extent of fingering, the previous focus has been on measuring the interfacial deformations or the finger length $\bar{\lambda}$. However, as evident in Fig. 3, the magnitude of $\bar{\lambda}$ is only millimetric in the weak fingering regime, which renders the boundary between weak and no fingering difficult to detect. More important, the true onset of particle-induced viscous fingering must be set by that of miscible fingering that initiates inside the suspension. In order to address this, we presently focus on the experiments at $h/d = 10.2$ only and compute the variance $S^2(r)$ [61] of the particle volume fraction in each pixel $\bar{\phi}_i$ at r from the average value $\bar{\phi}(r)$. The expression for $S^2(r)$ is given by

$$S^2(r) = \frac{1}{N-1}\sum_{i=1}^{N}[\bar{\phi}_i - \bar{\phi}(r)]^2, \tag{4}$$

where N is the total number of pixels from $\theta = 0$ to 2π at given r. While we expect $S^2(r)$ to be nonzero due to the pixel-level noise, its value must increase substantially when axisymmetry in the particle concentration breaks upon miscible fingering and the formation of particle clusters. This is clearly illustrated in the plot of $S^2(r)$ for $\phi_0 = 0.28$ (weak fingering) in contrast to that for $\phi_0 = 0.20$ (no fingering) in Fig. 6(a). There is a significant rise in $S^2(r)$ for $\phi_0 = 0.28$ at the radial position where miscible fingering visually initiates [see Fig. 6(b)], whereas $S^2(r)$ remains small and relatively constant in the $\phi_0 = 0.20$ case. Hence, computing S^2 for all experiments at $h/d = 10.2$ allows us to determine the range of ϕ_0 over which miscible fingering is observed, as well as the location and time at which miscible fingering first initiates.

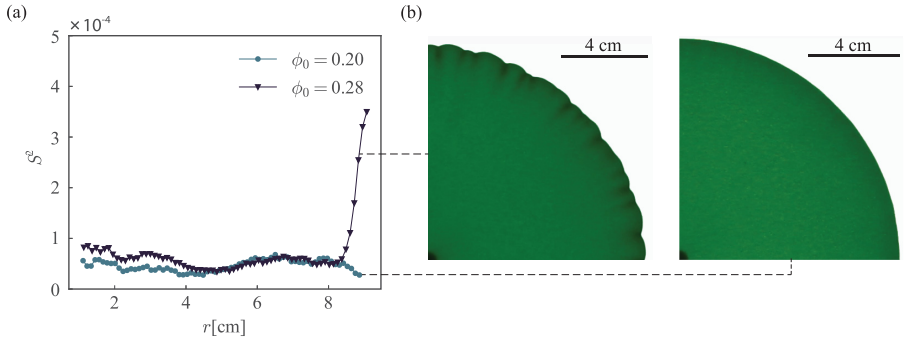

FIG. 6. (a) The plot of sample variance S^2 for $\phi_0 = 0.28$, $h/d = 10.2$ (weak fingering) and $\phi_0 = 0.20$, $h/d = 10.2$ (no fingering) at $t = 16$ s. Here, S^2 corresponds to the deviation of the particle concentration in each pixel $\bar{\phi}_i$ at given r from the average value $\bar{\phi}(r)$ and is a measure of axisymmetry breaking due to miscible fingering. For $\phi_0 = 0.28$, S^2 rises substantially close to the interface where miscible fingering occurs, while S^2 for $\phi_0 = 0.20$ remains small. (b) Corresponding experimental images for $\phi_0 = 0.28$ (left) and $\phi_0 = 0.20$ (right) confirm the effectiveness of S^2 in determining the onset of miscible fingering.

A. Onset of miscible fingering: Minimum viscosity gradient

In addition to S^2, we also compute the effective suspension viscosity μ_s based on $\bar{\phi}(r)$ to uncover the destabilizing viscosity gradient necessary for miscible fingering. The empirical expression for $\mu_s(\bar{\phi})$ [62] is given by

$$\frac{\mu_s(\bar{\phi})}{\mu_1} = 1 + \frac{2.5\phi_{\rm m}^2}{\phi_{\rm m} - \bar{\phi}} + \frac{0.1\bar{\phi}^2}{(\phi_{\rm m} - \bar{\phi})^2}, \tag{5}$$

where $\phi_{\rm m} \approx 0.59$ is the maximum packing fraction. Figure 7 shows the plot of $\mu_s[\bar{\phi}(r)]$ normalized by $\mu_s(\phi_0)$ as a function of $r/R(t)$ for $\phi_0 = 0.28$ and for $\phi_0 = 0.20$. For both cases, $\mu_s[\bar{\phi}(r)]/\mu_s(\phi_0)$ rises more steeply toward $r/R = 1$ over time, which directly corresponds to the temporal rise in particle accumulation at the interface. More important, even for $\phi_0 = 0.20$ in which no miscible fingering is observed, $\mu_s' > 0$, where the prime denotes the derivative with respect to $r/R(t)$. Therefore, a

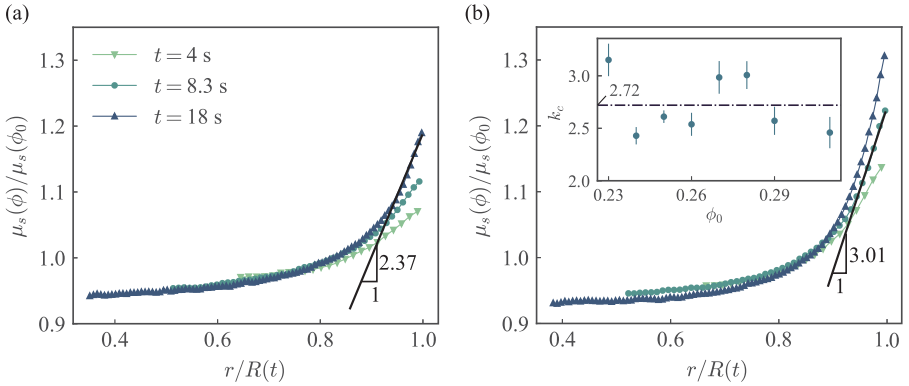

FIG. 7. The plot of the normalized effective viscosity $\mu_s(\bar{\phi})/\mu_s(\phi_0)$ over r/R for (a) $\phi_0 = 0.20$, $h/d = 10.2$ (no fingering) and (b) $\phi_0 = 0.28$, $h/d = 10.2$ (weak fingering). Because of particle accumulation, $\mu_s(\bar{\phi})/\mu_s(\phi_0)$ is shown to grow more steeply over time for both cases. In particular, we focus on the slope of the viscosity near the interface $k_c \approx 3$ at the onset of miscible fingering ($t = 8.3$ s). On average, this critical slope is measured to be about 2.7 for all $\phi_0 \geqslant 0.23$ for which miscible fingering is observed [inset of panel (b)].

nonzero viscosity gradient, $\mu_s' > 0$, alone is an insufficient condition for miscible fingering. It is important to acknowledge that, given the time-dependent nature of the radial flow, miscible fingering may develop over time even in the $\phi_0 = 0.20$ case. However, we presently focus on the onset of miscible fingering within the timescale of the experiments.

Then, does there exist a minimum destabilizing viscosity gradient that needs to be satisfied across all experiments? To address this question, we focus on the plot of $\mu_s(\bar{\phi})/\mu_s(\phi_0)$ specifically at the onset time of miscible fingering [$t = 8.3$ s in Fig. 7(b)], which was identified using S^2. The value of $\mu_s'/\mu_s(\phi_0)$ near the interface is measured to be approximately 3.0 for $\phi_0 = 0.28$. Notably, this value is higher than the largest slope ($\sim$2.4) achieved in $\phi_0 = 0.20$ with no miscible fingering [final time, $t = 18$ s, in Fig. 7(a)]. We hereby denote the largest slope at the time of miscible fingering as k_c and extract its value for all $\phi_0 \geqslant 0.23$. The result is included in the inset of Fig. 7(b) and demonstrates that k_c does not strongly vary with ϕ_0. In fact, within the reasonable margin of error, $k_c \sim 2.7$, independent of ϕ_0; this consistency in k_c is even more noteworthy, given that the onset time of miscible fingering (from which k_c is extracted) decreases with increasing ϕ_0. This strongly suggests the existence of the minimum viscosity gradient necessary for miscible fingering that is independent of ϕ_0 and the onset time.

Similarly, the concept of critical mobility ratio was previously explored in miscible fingering of pure liquids, when liquid with viscosity μ_{in} is injected into that of $\mu_{\text{out}} > \mu_{\text{in}}$ [63–65]. Lajeunesse *et al.* [63,64] first demonstrated that the viscosity ratio between the invading and defending fluids, or $\mu_{\text{in}}/\mu_{\text{out}}$, needs to be smaller than a critical value before miscible fingering is observed, which was confirmed more recently by Bischofberger and colleagues [65]. In our current study, because the effective viscosity varies continuously inside the suspension, the viscosity gradient $\mu_s'/\mu_s(\phi_0)$ is much more practical to extract over the mobility ratio. While the inverse of $\mu_{\text{in}}/\mu_{\text{out}}$ is conceptually analogous to the minimum viscosity gradient k_c, important differences exist. Namely, k_c is equivalent to the normalized *difference* in "defending" and "invading" viscosities over a spatial increment, as opposed to the *ratio* of viscosities. In addition, k_c, by definition, captures how sharply or gradually the effective viscosity varies, which may be an important advantage, as the sharpness of miscible interface between the two fluids was found to be a key parameter separating the stable from unstable regimes in Refs. [63–65]. In fact, in their model study of miscible fingering with a nonmonotonic viscosity profile, Manickam and Homsy [66,67] showed that both the magnitude of the viscosity ratio and how sharply it occurs play important roles in determining stability.

In order to understand the emergence of $k_c > 0$, we must consider key physical factors that act to delay or suppress miscible fingering in our current system. One hypothesis is that the stabilizing viscosity ratio between the suspension and air may counterbalance the destabilizing viscosity gradient inside the suspension, delaying the fingering onset and setting $k_c > 0$. Manickam and Homsy [66,67] found that, in the presence of nonmonotonic viscosity profile, the key physical mechanism of instability is the relative strength of locally unstable (upstream) and stable (downstream) flow regions, subject to diffusion. The interaction of locally stable and unstable viscosity contrasts that governs the global stability was also considered numerically by De Wit *et al.* [68]. In the present system, the destabilizing viscosity gradient is slightly upstream of the suspension-air interface across which the viscosity contrast is stable to fingering. Therefore, depending on the relative strength of two competing viscosity ratios, the unstable region inside the suspension may give rise to instability, if given sufficient time to develop within the timescale of our experiments.

Distinct from the aforementioned studies on miscible fingering [63–68], the current system also consists of an immiscible interface with surface tension, providing an additional "barrier" to instability. We have recently employed the linear stability analysis to successfully predict the critical wavelength of band fingering by including the surface tension effects of the suspension-air interface (manuscript in preparation). Therefore, we believe that the presence of the stabilizing suspension-air interface (both in the viscosity ratio and surface tension) may reasonably delay or completely suppress miscible fingering in our present experiments, unless the destabilizing viscosity

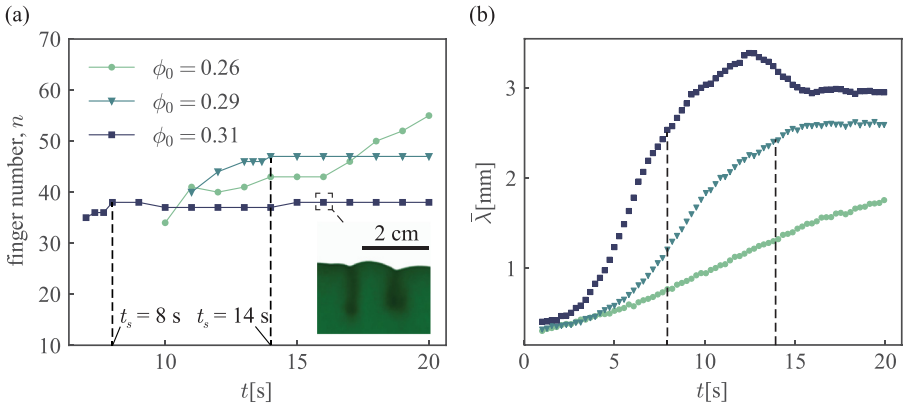

FIG. 8. (a) Once the interfacial finger forms between particle clusters (see the inset image), the number of fingers n may increase over time. This increase in n with time is evident in the plot of n vs t for $\phi_0 = 0.26$. However, for $\phi_0 = 0.29$ and 0.31, n exhibits an initial increase in time, until it plateaus to a constant value at the saturation time $t_s = 14$ and 8 s, respectively. (b) For $\phi_0 = 0.29$ and 0.31 at which the finger number saturates, the finger length $\bar{\lambda}$ is also shown to plateau after t_s; $\bar{\lambda}$ gradually increases on the timescale of the experiment for $\phi_0 = 0.26$.

gradient inside the suspension exceeds a critical value, or $k_c \sim 2.7$. Testing this present hypothesis will require a quantitative model comparing different physical effects, which we plan to develop in the near future.

B. Saturation in finger growth

We now consider the evolution of interfacial deformations as the result of miscible fingering and particle clustering inside the suspension. Once particle clusters form inside the suspension, the fluid-fluid interface fingers between the adjacent clusters, as shown in the inset of Fig. 8(a). Hence, following the onset of miscible fingering, we expect the number of interfacial fingers, n, to be nonzero and to grow over time as the suspension-air interface radially expands. To illustrate this, Fig. 8(a) shows the the time evolution of n for three different values of $\phi_0 > 0.25$. Overall, the number of interfacial fingers decreases with increasing ϕ_0, which alludes to the correlation between the most unstable wavelength and ϕ_0. More interestingly, for $\phi_0 = 0.29$ and 0.31, n is shown to plateau to constant values at $t_s = 14$ and 8 s, respectively, while n keeps growing for $\phi_0 = 0.26$ on the timescale of the experiment. The corresponding saturation behavior is also observed in the finger length, as $\bar{\lambda}$ plateaus over time to a constant value for $\phi_0 = 0.29$ and 0.31 in Fig. 8(b). Particularly for $\phi_0 = 0.29$, the time of saturation for $\bar{\lambda}$ is shown to closely match that of n. For $\phi_0 = 0.26$, $\bar{\lambda}$ exhibits a gradual increase with no sign of plateau, paralleling the gradual increase of n.

This time-independent behavior of finger growth for sufficiently large ϕ_0 is surprising, as the current system is inherently time dependent due to the continually expanding interface, $R(t)$. While the physics behind this saturation remains a topic of future studies, our present conjecture is that the saturation behavior is tied to the saturation of the volume fraction inside the particle clusters. Once the particle volume fraction in clusters reaches the maximum packing fraction (feasible for large ϕ_0), it may prevent the formation of additional particle clusters over time and hence justify the plateau in n. Finally, this saturation behavior is reminiscent of the nonlinear growth regime in miscible fingering of pure liquids [65,69], while being distinct. Bischofberger and colleagues [65,69] demonstrated that miscible fingers in some regime exhibit "proportionate growth"; proportionate growth refers to the growth of multiple length scales at the same rate so that the overall geometry is preserved. By contrast, the finger length over the suspension radius, $\bar{\lambda}/R(t)$, changes in our current study, as $\bar{\lambda}$ becomes constant over time. Despite the key differences, these conceptual similarities between

particle-induced viscous fingering and miscible fingering in liquids are noteworthy and may bring fundamental insight behind both systems.

IV. SUMMARY AND OUTLOOK

In this paper composed of two parts, we focus on the instability at the suspension-air interface when the mixture of oil and noncolloidal particles displaces air inside a Hele-Shaw cell. Termed particle-induced viscous fingering, this instability originates from miscible fingering inside the suspension, which, in turn, is caused by the accumulation of particles on the interface. In the first part of the paper, we review the experimental findings of Refs. [49,50] in which three distinct regimes ("no fingering," "weak fingering," and "band fingering") have been identified in terms of the particle volume fraction ϕ_0 and the channel gap size relative to the particle diameter, h/d. In addition to measuring the interfacial deformations, or finger length, we review how shear-induced migration across streamlines can lead to meniscus enrichment; this is the bare minimum condition required for particle-induced fingering to occur. The difference between gradual versus sharp particle accumulation is also rationalized based on the scaling analysis of a fountain flow near the interface.

While the previous work [49,50] has resolved many of the experimental observations, a fundamental question remains regarding the clear gap between the onset of particle accumulation and that of miscible fingering inside the suspension. In the second part of the paper, we address this question with new experimental results, focusing on the continuum limit ($h/d > 10$) for simplicity. We find that the nonzero viscosity gradient set by particle accumulation is clearly insufficient to cause miscible fingering in suspensions. We then extract the value of the critical viscosity gradient ($\sim$2.7) at the onset of miscible fingering, which appears to be fairly consistent across all ϕ_0. This minimum viscosity gradient is conceptually analogous to the critical mobility ratio that was previously identified in miscible fingering of pure liquids [63–65]. In addition, the growth of interfacial fingers that form as a result of miscible fingering is shown to "saturate" both in length and number for dense suspensions, while the suspension radius continues to grow in time. This behavior is in clear contrast to miscible fingers between pure liquids that grow at the same rate as the expanding radius [65,69].

Many questions remain especially in light of the experimental results in Sec. III. For instance, the physical mechanisms behind the minimum viscosity gradient and the saturation in finger growth are currently not well understood, presenting opportunities for model development. More important, the similarities and clear differences that have emerged between miscible fingering in suspensions versus liquids warrant detailed analysis. Furthermore, modulating particle properties, such as the wettability, shape, and buoyancy, has the potential to completely change the macrosopic phenomena and is of great interest for future studies. Going back to the previous work [49,50], the correlation between ϕ_0 and the unstable wavelength and even the mechanism of particle accumulation in the limit of $h \to d$ remain unresolved. Additional challenges include mathematical modeling and improved experimental visualization of interfacial dynamics of dense suspensions, especially with decreasing h/d.

Despite remaining questions and the narrow scope of the present study, one simple fact stands: Modification of the effective viscosity with suspended particles is a simple yet extremely powerful tool to changing the interfacial dynamics. In particular, generating the gradient in viscosity with nonhomogeneous particle distributions can naturally lend itself to scenarios that are either stable or unstable to viscous fingering. The change in effective viscosity is only one way that suspended particles affect the bulk rheology, as the inclusion of particles in a Newtonian liquid are known to incur more complex rheological changes particularly at high particle concentrations. Hence, the intersection of bulk suspension rheology and the interfacial dynamics holds great promise for yielding rich fluid mechanics phenomena that may have been observed but not yet been carefully considered.

ACKNOWLEDGMENT

The authors would like to thank Michael P. Brenner for guidance and helpful discussions.

[1] J. J. Stickel and R. L. Powell, Fluid mechanics and rheology of dense suspensions, Annu. Rev. Fluid Mech. **37**, 129 (2005).
[2] M. M. Denn and J. F. Morris, Rheology of non-Brownian suspensions, Annu. Rev. Chem. Biomol. **5**, 203 (2014).
[3] D. Leighton and A. Acrivos, Measurement of shear-induced self-diffusion in concentrated suspensions of spheres, J. Fluid Mech. **177**, 109 (1987).
[4] D. Leighton and A. Acrivos, The shear-induced migration of particles in concentrated suspensions, J. Fluid Mech. **181**, 415 (1987).
[5] É. Guazzelli and J. F. Morris, *A Physical Introduction to Suspension Dynamics* (Cambridge University Press, Cambridge, UK, 2012).
[6] R. J. Phillips, R. C. Armstrong, R. A. Brown, A. L. Graham, and J. R. Abbott, A constitutive equation for concentrated suspensions that accounts for shear-induced particle migration, Phys. Fluids **4**, 30 (1992).
[7] F. Boyer, É. Guazzelli, and O. Pouliquen, Unifying Suspension and Granular Rheology, Phys. Rev. Lett. **107**, 188301 (2011).
[8] H. A. Barne, Shear-thickening ("dilatancy") in suspensions of nonaggregating solid particles dispersed in Newtonian liquids, J. Rheol. **33**, 329 (1989).
[9] N. J. Wagner and J. F. Brady, Shear thickening in colloidal dispersions, Phys. Today **62**, 27 (2009).
[10] E. Brown, N. A. Forman, C. S. Orellana, H. Zhang, B. W. Maynor, D. E. Betts, J. M. DeSimone, and H. M. Jaeger, Generality of shear thickening in dense suspensions, Nat. Mater. **9**, 220 (2010).
[11] R. Seto, R. Mari, J. F. Morris, and M. M. Denn, Discontinuous Shear Thickening of Frictional Hard-Sphere Suspensions, Phys. Rev. Lett. **111**, 218301 (2013).
[12] R. Mari, R. Seto, J. F. Morris, and M. M. Denn, Shear thickening, frictionless and frictional rheologies in non-Brownian suspensions, J. Rheol. **58**, 1693 (2014).
[13] I. R. Peters, S. Majumdar, and H. M. Jaeger, Direct observation of dynamic shear jamming in dense suspensions, Nature (London) **532**, 214 (2016).
[14] N. Y. C. Lin, C. Ness, M. E. Cates, J. Sun, and I. Cohen, Tunable shear thickening in suspensions, Proc. Natl. Acad. Sci. USA **113**, 10774 (2016).
[15] F. Boyer, O. Pouliquen, and É. Guazzelli, Dense suspensions in rotating-rod flows: Normal stresses and particle migration, J. Fluid Mech. **686**, 5 (2011).
[16] A. S. Wineman and A. C. Pipkin, Slow viscoelastic flow in tilted troughs, Acta Mech. **2**, 104 (1966).
[17] R. I. Tanner, Some methods for estimating the normal stress functions in viscometric flows, Trans. Soc. Rheol. **14**, 483 (1970).
[18] É. Couturier, F. Boyer, O. Pouliquen, and É. Guazzelli, Suspensions in a tilted trough: Second normal stress difference, J. Fluid Mech. **686**, 26 (2011).
[19] R. J. Furbank and J. F. Morris, An experimental study of particle effects on drop formation, Phys. Fluids **16**, 1777 (2004).
[20] R. J. Furbank and J. F. Morris, Pendant drop thread dynamics of particle-laden liquids, Int. J. Multiphas. Flow **33**, 448 (2007).
[21] C. Bonnoit, T. Bertrand, E. Clément, and A. Lindner, Accelerated drop detachment in granular suspensions, Phys. Fluids **24**, 043304 (2012).
[22] T. Bertrand, C. Bonnoit, E. Clément, and A. Lindner, Dynamics of drop formation in granular suspensions: The role of volume fraction, Granular Matter **14**, 169 (2012).
[23] M. Z. Miskin and H. M. Jaeger, Droplet formation and scaling in dense suspensions, Proc. Natl. Acad. Sci. USA **109**, 4389 (2012).

[24] M. S. van Deen, T. Bertrand, N. Vu, D. Quéré, E. Clément, and A. Lindner, Particles accelerate the detachment of viscous liquids, Rheol. Acta **52**, 403 (2013).
[25] J. Zhou, B. Dupuy, A. L. Bertozzi, and A. E. Hosoi, Theory for Shock Dynamics in Particle-Laden Thin Films, Phys. Rev. Lett. **94**, 117803 (2005).
[26] T. Ward, C. Wey, R. Glidden, A. E. Hosoi, and A. L. Bertozzi, Theory for shock dynamics in particle-laden thin films, Phys. Fluids **21**, 083305 (2009).
[27] B. P. Cook, Theory for particle settling and shear-induced migration in thin-film liquid flow, Phys. Rev. E **78**, 045303 (2008).
[28] N. Murisic, J. Ho, V. Hu, P. Latterman, T. Koch, K. Lin, M. Mata, and A. L. Bertozzi, Particle-laden viscous thin-film flows on an incline: Experiments compared with an equilibrium theory based on shear-induced migration and particle settling, Physica D (Amsterdam, Neth.) **240**, 1661 (2011).
[29] N. Murisic, B. Pausader, D. Peschka, and A. L. Bertozzi, Dynamics of particle settling and resuspension in viscous liquid films, J. Fluid Mech. **717**, 203 (2013).
[30] A. Mavromoustaki and A. L. Bertozzi, Hyperbolic systems of conservation laws in gravity-driven, particle-laden thin-film flows, J. Eng. Math. **88**, 29 (2014).
[31] L. Wang and A. L. Bertozzi, Shock solutions for high concentration particle-laden thin films, SIAM J. Math. Anal. **74**, 322 (2014).
[32] S. Lee, Y. Stokes, and A. L. Bertozzi, Behavior of a particle-laden flow in a spiral channel, Phys. Fluids **26**, 043302 (2014).
[33] S. Lee, A. Mavromoustaki, G. Urdaneta, K. Huang, and A. L. Bertozzi, Experimental investigation of bidensity slurries on an incline, Granular Matter **16**, 269 (2014).
[34] S. Lee, J. Wong, and A. L. Bertozzi, Equilibrium theory of bidensity particle-laden flows on an incline, in *Mathematical Modelling and Numerical Simulation of Oil Pollution Problems*, edited by M. Ehrhardt (Springer, Berlin, 2015).
[35] M. Kulkarni, S. Sahoo, P. Doshi, and A. V. Orpe, Fingering instability of a suspension film spreading on a spinning disk, Phys. Fluids **28**, 063303 (2016).
[36] E. H. Mansfield, H. R. Sepangi, and E. A. Eastwood, Equilibrium and mutual attraction or repulsion of objects supported by surface tension, Philos. Trans. R. Soc. London, Ser. A **355**, 868 (1997).
[37] P. A. Kralchevsky and K. Nagayama, Capillary interactions between particles bound to interfaces, liquid films, and biomembranes, Adv. Colloid Interfac. **85**, 145 (2000).
[38] B. P. Binks, Particles as surfactants—similarities and differences, Curr. Opin. Colloid Interface **7**, 21 (2002).
[39] D. Vella, H.-Y. Kim, P. Aussillous, and L. Mahadevan, Dynamics of Surfactant-Driven Fracture of Particle Rafts, Phys. Rev. Lett. **96**, 178301 (2006).
[40] C. Planchette, E. Lorenceau, and A. L. Biance, Surface wave on particle raft, Soft Matter **8**, 2444 (2012).
[41] S. U. Pickering, CXCVI—Emulsions, J. Chem. Soc., Trans. **91**, 2001 (1907).
[42] A. B. Subramaniam, M. Abkarian, L. Mahadevan, and H. A. Stone, Colloid science: Non-spherical bubbles, Nature (London) **438**, 930 (2005).
[43] A. B. Subramaniam, M. Abkarian, and H. A. Stone, Controlled assembly of jammed colloidal shells on fluid droplets, Nat. Mater. **4**, 553 (2005).
[44] M. Abkarian, S. Protière, J. M. Aristoff, and H. A. Stone, Gravity-induced encapsulation of liquids by destabilization of granular rafts, Nat. Commun. **4**, 1895 (2013).
[45] P. Aussillous and D. Quéré, Liquid marbles, Nature (London) **411**, 924 (2001).
[46] Y. Timounay, O. Pitois, and F. Rouyer, Gas Marbles: Much Stronger than Liquid Marbles, Phys. Rev. Lett. **118**, 228001 (2017).
[47] H. Tang, W. Grivas, D. Homentcovschi, J. Geer, and T. Singler, Stability Considerations Associated with the Meniscoid Particle Band at Advancing Interfaces in Hele-Shaw Suspension Flows, Phys. Rev. Lett. **85**, 2112 (2000).
[48] A. Ramachandran and D. T. Leighton, Particle migration in concentrated suspensions undergoing squeeze flow, J. Rheol. **54**, 563 (2010).
[49] F. Xu, J. Kim, and S. Lee, Particle-induced viscous fingering, J. Non-Newton. Fluid **238**, 92 (2016).

[50] J. Kim, F. Xu, and S. Lee, Formation and Destabilization of the Particle Band on the Fluid-Fluid Interface, Phys. Rev. Lett. **118**, 074501 (2017).
[51] G. M. Homsy, Viscous fingering in porous media, Annu. Rev. Fluid Mech. **19**, 271 (1987).
[52] C. Chevalier, A. Lindner, and E. Clément, Destabilization of a Saffman-Taylor Fingerlike Pattern in a Granular Suspension, Phys. Rev. Lett. **99**, 174501 (2007).
[53] Ø. Johnsen, C. Chevalier, A. Lindner, R. Toussaint, E. Clément, K. J. Måløy, E. G. Flekkøy, and J. Schmittbuhl, Decompaction and fluidization of a saturated and confined granular medium by injection of a viscous liquid or gas, Phys. Rev. E **78**, 051302 (2008).
[54] C. Chevalier, A. Lindner, M. Leroux, and E. Clément, Morphodynamics during air injection into a confined granular suspension, J. Non-Newton. Fluid **158**, 63 (2009).
[55] B. Sandnes, E. G. Flekkoy, H. A. Knudsen, K. J. Maloy, and H. See, Patterns and flow in frictional fluid dynamics, Nat. Commun. **2**, 288 (2011).
[56] A. Karnis and S. G. Mason, The flow of suspensions through tubes. IV. Meniscus effects, J. Colloid Interf. Sci. **23**, 120 (1967).
[57] S. Bhattacharji and P. Savic, Real and apparent non-Newtonian behavior in viscous pipe flow of suspensions driven by a fluid piston, in *Proceedings of the 1965 Heat Transfer and Fluid Mechanics Institute*, University of California, Los Angeles, edited by Andrew F. Charwat (Stanford University Press, Palo Alto, CA, 1965).
[58] Y. Shan, M. Normand, and M. Peleg, Estimation of the surface concentration of adhered particles by colour imaging, Powder Technol. **92**, 147 (1997).
[59] P. R. Nott and J. F. Brady, Pressure-driven flow of suspensions: Simulation and theory, J. Fluid Mech. **275**, 157 (1994).
[60] B. Snook, J. E. Butler, and É. Guazzelli, Dynamics of shear-induced migration of spherical particles in oscillatory pipe flow, J. Fluid Mech. **786**, 128 (2016).
[61] S. M. Ross, *Introduction to Probability and Statistics for Engineers and Scientists* (Academic Press, San Diego, 2014).
[62] J. F. Morris and F. Boulay, Curvilinear flows of noncolloidal suspensions: The role of normal stresses, J. Rheol. **43**, 1213 (1999).
[63] E. Lajeunesse, J. Martin, N. Rakotomalala, and D. Salin, 3d Instability of Miscible Displacements in a Hele-Shaw Cell, Phys. Rev. Lett. **79**, 5254 (1997).
[64] E. Lajeunesse, J. Martin, N. Rakotomalala, D. Salin, and Y. C. Yortsos, Miscible displacement in a Hele-Shaw cell at high rates, J. Fluid Mech. **398**, 299 (1999).
[65] I. Bischofberger, R. Ramachandran, and S. R. Nagel, Fingering versus stability in the limit of zero interfacial tension, Nat. Commun. **5**, 5265 (2014).
[66] O. Manickam and G. M. Homsy, Stability of miscible displacements in porous media with nonmonotonic viscosity profiles, Phys. Fluids A **5**, 1356 (1993).
[67] O. Manickam and G. M. Homsy, Simulation of viscous fingering in miscible displacements with nonmonotonic viscosity profiles, Phys. Fluids **6**, 95 (1994).
[68] A. De Wit, Y. Bertho, and M. Martin, Viscous fingering of miscible slices, Phys. Fluids **17**, 054114 (2005).
[69] I. Bischofberger, R. Ramachandran, and S. R. Nagel, An island of stability in a sea of fingers: Emergent global features of the viscous-flow instability, Soft Matter **11**, 7428 (2015).